

Biodegradable PLA/PBAT/Clay Nanocomposites: Morphological, Rheological and Thermomechanical Behavior

Juan P. Correa^{1,2*}, Alejandro Bacigalupe^{2,3}, Jorge Maggi⁴ and Patricia Eisenberg^{2,3}

¹National Council of Scientific and Technical Research, Av. Rivadavia 1917, Buenos Aires, Argentina

²National University of San Martín – UNSAM 3iA, Campus Miguelete, Av. 25 de Mayo y Francia, San Martín, Buenos Aires, Argentina

³National Institute of Industrial Technology, Av. Gral. Paz 5445, San Martín, Buenos Aires, Argentina

⁴Technology Center of Mineral Resources and Ceramics, Cno. Centenario y 506, La Plata, Buenos Aires, Argentina

Received February 29, 2016; Accepted May 27, 2016

ABSTRACT: Poly(lactic acid)/poly(butylene adipate-co-terephthalate) (PLA/PBAT)-based nanocomposites were prepared by melt blending of PLA and PBAT with 5 wt% of unmodified (Cloisite Na) and modified (Cloisite 30B) montmorillonites. X-ray diffraction (XRD) revealed an intercalated structure in both nanocomposites. The extent of the intercalation was higher for nanocomposites based on modified clays (OMMT) with chemical affinity with the polymer matrix. Rheological measurements have shown an increase in viscosity and a better degree of clay dispersion for nanocomposites containing OMMT. Nanocomposites with OMMT showed lower PBAT separated phase particle size and improvements in thermal stability, mechanical properties and water vapor barrier when compared with the neat blend. Finally, our results showed that the organically modified clay has a higher affinity than natural clay with the studied polymer blend.

KEYWORDS: Poly(lactic acid), poly(butylene adipate-co-terephthalate), nanocomposites, clays, montmorillonite

1 INTRODUCTION

Poly(lactic acid) (PLA) is an aliphatic polyester produced from renewable resources and one of the most promising biodegradable materials because of its good physical properties, such as high mechanical strength, transparency, and printability; and on account of its being easily processed with the machines and equipment used in the processing of other plastic materials. However, some characteristics of PLA, like fragility, rigidity and the possibility of its degradation during processing due to low thermal stability, are restricting the range of applications as a commodity polymer [1]. One strategy to overcome these drawbacks is the development of polymer blends of PLA with other biodegradable polymers with higher flexibility, toughness and thermal stability like poly(butylene adipate-co-terephthalate) (PBAT) [2]. On the other hand, the formulation of polymers with clays (as montmorillonites or MMT) with a lower clay content in nanocomposites (1–5% by weight), is also associated with an improvement in the thermomechanical,

rheological and barrier properties [3]. In fact, Gunning *et al.* [4] and Yu *et al.* [5] have found that the optimum level of clay loading to reinforce a PLA matrix and a PLA/polycaprolactone blend respectively is 5% w/w. There are currently several applications for these nanocomposites such as car parts (safety belts, engine parts) and packaging for cosmetics, food, medicine, electronics, films and bottles, among others [3]. Regarding PLA/PBAT-based nanocomposites, very few studies have reported the addition of clays in this polymer blend to obtain nanocomposites, and surprisingly, only PLA with low flow capability (extrusion grade) was used in all of them [6–8]. The aim of this study was to develop polymer/MMT nanocomposites using a biodegradable polymer blend with a high content of renewable polymer with high flow capability (injection molding grade PLA), and to understand the effect of the high flow capability of PLA and the type of MMT (unmodified or organically modified) on the intercalation of polymeric chains into clay galleries and on the final properties of the biodegradable nanocomposite.

*Corresponding author: jcorrea@inti.gob.ar

2 EXPERIMENTAL SECTION

2.1 Materials

As reference, PLA Ingeo™ 3251D (injection grade or PLA through the paper) with a melt flow index of 35 g/10 min (190 °C, 2.16 kg) and 7001D (extrusion grade or PLA-ext; in Section 3.1) with a melt flow index of 6 g/10 min (190 °C, 2.16 kg) were obtained from NatureWorks in the form of pellets. PBAT Ecoflex® F Blend A1200 was obtained from BASF in the form of pellets with a melt flow index of 2.7–4.9 g/10 min (190 °C, 2.16 kg). Two grades of montmorillonite clay (MMT) under the commercial names of Cloisite Na (unmodified MMT) and Cloisite 30B (organically modified montmorillonite or OMMT) were used. The characteristics and notation of these clays in the text are listed in Table 1.

2.2 Preparation of Nanocomposite Films

Prior to mixing PLA, PBAT and clays were dried under vacuum at 80 °C during 8 hours. Nanocomposites were prepared via melt intercalation in an internal mixing chamber of a Brabender Plasti-Corder (30 cm³). The mixing was performed at 180 °C, with a rotor speed of 60 rpm for 8 minutes. Nanocomposite blends with a content of PLA 80/PBAT 20 (% w/w) and a MMT fixed content of 5% w/w were prepared. In this work, the PLA/PBAT blend of 80/20 (% w/w) was the proportion selected because it was the blend with the highest content of renewable polymer (PLA) without detrimental consequences on processability due to the high melt index of the injection grade PLA. The nanocomposites obtained were labeled as PLA/PBAT/MMT (80/20/MMT). The same mixing procedure was used to obtain neat PLA, PBAT, and a PLA/PBAT blend (80/20% w/w) for comparison. Films of the different samples were obtained by compression molding at 190 °C using an 8 minute molding cycle. All characterizations were made on 0.2 to 0.3 mm thick films.

2.3 Nanocomposite Characterization

Clays, neat polymers and their nanocomposite structures were evaluated with X-ray diffraction (XRD).

XRD patterns were taken with a Phillips PW 1730/10 X-ray diffractometer, operated at 40 kV and 30 mA, equipped with Cu K α radiation at a 0.1546 nm wavelength. Diffraction data was collected over a 2 θ range of 2°–10°, with a step width of 0.02° and a counting time of 2.0 seconds/step. Basal spacing (d_{001}) of the clay layer was calculated using the Bragg's equation:

$$\lambda = 2d \sin \theta \quad (1)$$

where λ is the wavelength of the X-ray radiation used (0.1546 nm), d is the spacing between diffractive planes and θ is the measured diffraction angle.

Viscoelastic properties were measured through an oscillatory rheometer (Physica MCR301, Anton Paar GmbH) equipped with plate-plate geometry of 50 mm diameter (PP50) at 180 °C. Frequency sweep tests were carried out at an angular velocity range of 0.01–500 s⁻¹ and 1% of strain (under the linear viscoelastic region). The test was repeated two times for each sample in order to obtain a representative value and average values were reported. Scanning electronic microscopy (SEM) was carried out on the cryogenic fracture surfaces of the samples using a Quanta FEG 250 microscope operating at a voltage between 4 to 10 kV. The samples were previously sputter-coated with gold to increase their electric conductivity. The cross-sectional diameters of the dispersed phase were measured using ImageJ 1.8v (Wayne Rasband, National Institutes of Health, USA). Determinations were performed in different areas of the SEM images.

Tensile testing was performed with an Instron Universal Testing Machine Model 5569. The tests were carried out at 23 °C, with a constant rate of 5 mm/min, an initial grip separation of 50 mm and ribbon-shape samples (10 mm width) according to ASTM D882-12 method [9].

Differential scanning calorimetry (DSC) tests were carried out using a Mettler 822 differential scanning calorimeter under nitrogen atmosphere at a scanning rate of 10 °C/min, with a sample of 10–11 mg in aluminium pans. The thermal history of the samples was erased by a preliminary heating cycle at 10 °C/min from 20 to 200 °C. The glass transition temperatures (T_g), cold crystallization temperatures (T_c) and melting temperatures (T_m) were determined from the second

Table 1 Characteristics of Montmorillonites used in this work.

Type of clay	Organic modifier	Modifier concentration (Meq/100g Clay)	Notation in text
Cloisite Na+	None	None	CNa
Cloisite 30B	$\begin{array}{c} \text{CH}_2\text{CH}_2\text{OH} \\ \\ \text{H}_3\text{C}-\text{N}^+-\text{T} \\ \\ \text{CH}_2\text{CH}_2\text{OH} \end{array}$	90	C30B

T = Tallow (~65% C18; ~30% C16; ~5% C14).

heating scan. The enthalpies of crystallization (ΔH_{cc}) and melting (ΔH_m) were normalized according to the proportion of components in the blends. The crystallinity (χ_c) was determined from Equation 2:

$$\chi_c = \frac{\Delta H}{\left[\Delta H_m^0 * (1 - w_{clay}) * (w_x) \right]} \quad (2)$$


where w_{clay} is the OMMT mass fraction, w_x is the fraction of each polymer of the blend, $\Delta H = \Delta H_m - \Delta H_{cc}$ (if corresponding) and ΔH_m^0 is the theoretical value of the melting enthalpy of crystalline polymers. These values are 93 J/g for PLA and 114 J/g for PBAT [7]. The oxidation onset temperatures (OOT) of samples were measured using the method described in ASTM E2009 and analyzed from 30 °C to 350 °C at a heating rate of 10 °C/min [10]. Water vapor permeability (WVP) of fabricated films was measured using the cups method described in ASTM E96/E96M-15 [11]. Measurements were carried out at 23 °C and 50% of relative humidity respectively. Three measurements were carried out for the neat polymers, 80/20 blend and its nanocomposites.

Tensile strength, dispersed phase size and WVP of films were subjected to analysis of variance (ANOVA), and the Tukey's test was applied at the 0.05 level of significance. All statistical analyses were performed using Minitab Statistical Software Release 12 (Pennsylvania, USA).

3 RESULTS AND DISCUSSION

3.1 X-ray Diffraction (XRD)

X-ray diffraction patterns of neat polymers, clays and nanocomposites are shown in Figure 1. Concerning the patterns, these were taken from $2\theta = 2$ to 10° because the most significant features of clay nanocomposites,

like the evolution of the basal spacing and dispersion state of clays (intercalation/exfoliation), are located in the lower angle range. CNa is characterized by a single diffraction peak at $2\theta = 7.95$, corresponding to the basal reflection (001), which results in an interlayer distance $d_{(001)}$ of 11.10 Å according to the Bragg equation. On the other hand, C30B is characterized by a larger diffraction peak at $2\theta = 4.94$, corresponding to a $d_{(001)}$ of 17.86 Å. This larger $d_{(001)}$ in the neat C30B is due to the insertion of the organic modifier between the clay layers (see Table 1). For the control samples (labeled as neat PLA, neat PBAT and 80/20), no noticeable XRD peaks were observed over the studied angles. Cna-d nanocomposite shows a slight shift of the clay diffraction peak to lower angles ($2\theta = 7.25$), which corresponds with an increase ($\Delta d_{(001)}$) of around 1 Å compared with pristine CNa. This peak movement to lower angles is related to the intercalation of polymeric chains inside clay layers. In the case of 80/20/C30B-based nanocomposite, a shift of the clay diffraction peak to lower angles also occurred ($2\theta = 2.49$). This larger peak shift corresponds to a $\Delta d_{(001)}$ of almost 17 Å and indicates a good interaction of C30B with the PLA/PBAT polymeric blend. The apparently higher intercalation of polymer chains inside clays observed upon the addition of OMMT was already reported in the literature for several polyester/clay nanocomposites and is related to the hydrogen bond interactions between the hydroxyl groups of the C30B organic modifier (Table 1) and the carbonyl groups of polyester chains [12–14]. The origin of the other peak around $2\theta = 4.54$ (only observed in 80/20/C30B nanocomposite) has been discussed by several authors. Yu *et al.* [5] studied PLA/polycaprolactone/OMMT nanocomposites and explained that small peaks located at $2\theta = 4.86$ are caused by the (002) plane (d_{002}) of the silicate layers dispersed in the polymer matrix. On the other hand, the onset decomposition temperature of the organic

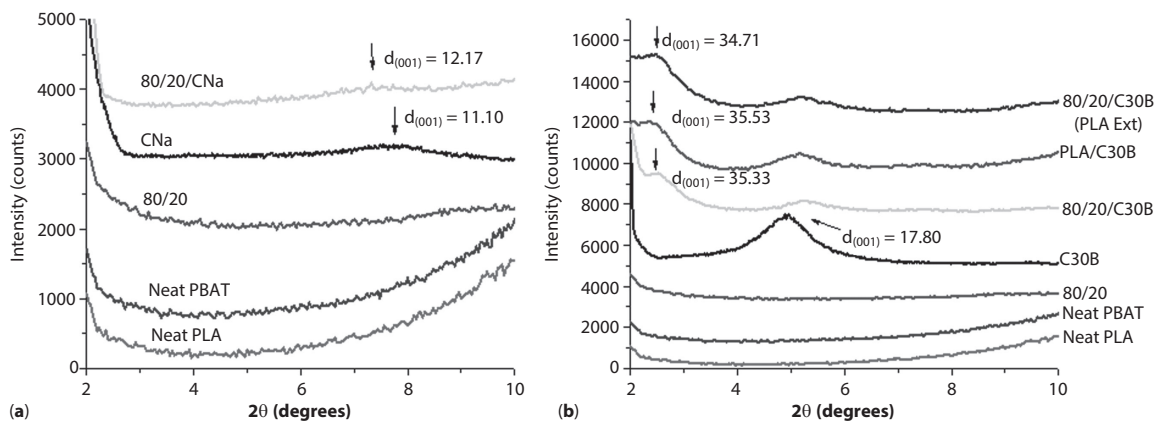


Figure 1 X-ray diffraction patterns of neat polymers, clays and nanocomposites.

modifier of C30B obtained by thermogravimetric analysis (TGA) was in the range of 174 to 200 °C according to Cervantes-Uc *et al.* [15] and Botana *et al.* [14] respectively. Considering that in this research, the mixing temperature during nanocomposites processing was 180 °C followed by thermocompression molding at 190 °C, the second peak located around $2\theta = 4.54$ may also be due to agglomeration of clay particles caused by thermal degradation of the organic modifier. On the other hand, Fornes *et al.* [16] studied the influence of the polymer matrix molecular weight (flow capability) on clay dispersion and properties of nylon 6/clay nanocomposites. They concluded that a high molecular weight nylon 6 (low flow) is consistently more effective at exfoliating OMMT during melt processing than the low molecular weight nylon 6 (high flow), due to the high shear stresses in the extruder that result from its high melt viscosity. In order to understand the effect of the PBAT addition and PLA flow capability on C30B dispersion, nanocomposites based on PLA/C30B (95/5% w/w) and a blend of PLA-ext/PBAT/C30B (80/20/5% w/w) were prepared following the same mixing process for DRX analysis (described in Section 2.2). For both samples, the shift of the clay diffraction peak to lower angles also produce a $\Delta d_{(001)}$ of around 17 Å compared with neat C30B. The results (also shown in Figure 1b) clearly indicate that PBAT addition to PLA and the PLA flow capability seems to have no effect on the extent of polymer intercalation into the clay galleries.

3.2 Rheological Measurement

Figure 2 shows complex viscosity values (η) in relation to the angular frequency (ω). PLA shows a pseudo-Newtonian behavior with nearly constant and low viscosity throughout the frequency range studied. In

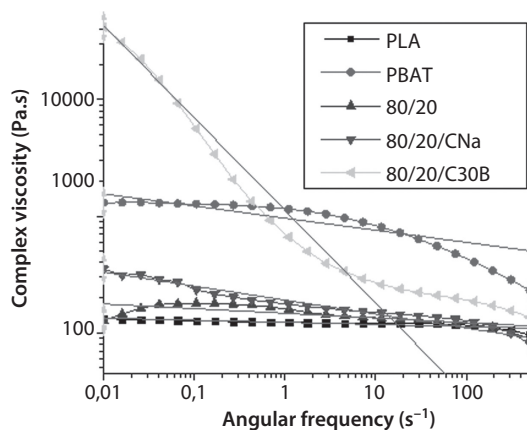


Figure 2 Complex viscosity values (η) in relation to the angular frequency (ω).

the case of PBAT, the complex viscosity decreases with the increase of angular frequency in a shear-thinning behavior. Complex viscosity values and behavior of both polymers are in agreement with those reported for PLA 3251D [17] and PBAT Ecoflex® [18]. On the other hand, formulation of PLA with PBAT and clays causes a shear-thinning behavior and an increase in complex viscosity of 1.5, 2 and around 46 times for 80/20, 80/20/CNa and 80/20/C30B respectively, using the frequency of 0.1 s⁻¹ as reference when compared with the one of the neat PLA. This increase in viscosity is due to the PBAT's higher viscosity and to the formation of interconnected structures between the polymer and the fillers [18, 19]. Furthermore, at high frequencies the viscosities of the nanocomposites are similar to the viscosity of the neat blend, suggesting that platelets are oriented in the flow direction due to applied shear force. The dispersion of nanoparticles in polymer matrices can also be studied through rheological analysis at a macroscopic scale [19]. The analysis of clay platelets dispersion can be achieved by adapting the complex viscosity curves (η^*) to the power law model (Equation 3).

$$\eta^* = A\omega^n \tag{3}$$

The n factor, which is related to the degree of clay dispersion into the matrix [19], was calculated by fitting the curve between 0.01 and 1 s⁻¹. The n value of 80/20/CNa tends to 0 and implies low intercalation of the polymer chains into the basal space of the clays. On the contrary, the n value for 80/20/C30B tends to 0.8, indicating a better intercalation/exfoliation degree [19]. Figure 3 presents storage modulus (G') in relation to ω . PLA, PBAT and 80/20 show strong liquid-like behavior ($G' \sim \omega^2$). Also, G' values for 80/20/CNa are very similar to those of the neat blend, indicating a low dispersion of the silicates in the matrix. On the contrary, 80/20/C30B blend possesses a solid-like

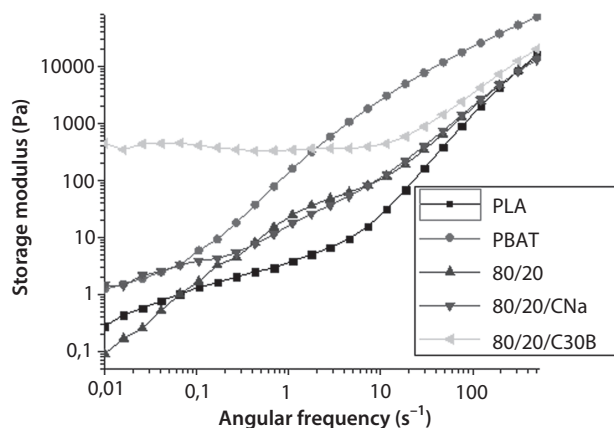


Figure 3 Storage modulus (G') in relation to ω .

behavior given by the plateau generated at low frequencies. This effect is attributed to the formation of a superstructure (percolated network) in the molten state, which influences the chain relaxation of the polymer. This structure only can be achieved with OMMT C30B and could also be another indicator of the better affinity of this clay with the polyesters blends and better intercalation/exfoliation degree of the clays inside the matrix [7, 19].

3.3 Scanning Electron Microscopy (SEM)

The SEM images of the freeze-fracture surfaces of the 80/20 blend and its nanocomposites are shown in Figure 4. The 80/20 blend micrograph (Figure 4a) shows a two-phase morphology in which the PBAT particles (minor component) are dispersed in the PLA matrix in accordance with what was previously reported for PLA Ingeo™ 2002D (extrusion grade)/PBAT Ecoflex® blends by Quero *et al.* [20]. Also, the images show that the interphase is well delineated in the blend, which is indicative of low adhesion between the PLA matrix and the PBAT particles. For

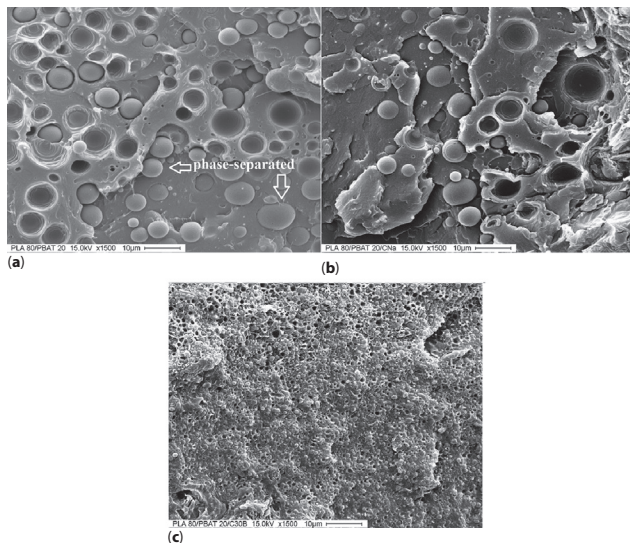


Figure 4 SEM images of the freeze-fracture surfaces of the 80/20 blend and its nanocomposites.

nanocomposites, some changes in their morphology were observed. The addition of C30B (Figure 4c) produces a coarser fracture surface compared to 80/20 and 80/20/CNa (Figure 4a,b) and a decrease (of around 80%) of the dispersed phase (PBAT) particle size. The PBAT dispersed phase diameters in the 80/20 blend and in the nanocomposites are summarized in Table 2. This domain size reduction phenomenon has been reported for several polymer blends [21, 22] and may be attributed to the reduction of coalescence in the system given by the compatibilizer role of the clay platelets in the blend. It is interesting to note that average size domains depend on the MMT type and the extent of intercalation. Particle size reduction was more effective for blends with C30B. These results were in agreement with those obtained by XRD and rheological measurements and show that among both clays used, the hydrophobic C30B exhibited the best interaction with the PLA/PBAT polymer blend.

3.4 Tensile Properties

The influence of PBAT and clays addition on the PLA tensile properties was evaluated. Results of the tensile properties for all formulations are also shown in Table 2. According to these results, PLA exhibits a high tensile strength (TS) and tensile modulus (E) but very low elongation at break (ϵ_b), while PBAT is a ductile material with a higher ϵ_b and lower E and TS values when compared to PLA. As expected, E and TS values of 80/20 blend decreased due to the PBAT addition, but no noticeable improvement in ϵ_b of the blend was observed. This effect could be due to the immiscibility of polymers and the low adhesion between PLA matrix and PBAT phase (see Figure 4a). Concerning nanocomposites, tensile modulus of 80/20/C30B was the only mechanical property improved (around 20%) by clay incorporation in comparison with 80/20 neat blend. In fact, clay addition leads to a decrease in the TS (16.5 and 14.4%) and ϵ_b (26.2 and 43.7%) in the case of 80/20/CNa and 80/20/C30B respectively when compared with PLA/PBAT neat blend. In this sense, Mohapatra *et al.* [8] studied the morphology and tensile properties of PLA Ingeo™ 4042D (extrusion

Table 2 Average domain size and tensile properties of all samples.

Sample	Domain size (μm)	Tensile Modulus (MPa)	Tensile Strength (MPa)	Elongation at break (%)
PBAT	–	75 ± 2^a	9.53 ± 0.55^a	250.34 ± 25.96^a
PLA	–	1611 ± 147^b	46.54 ± 7.03^b	4.06 ± 0.47^b
80/20	8.86 ± 1.08^a	1352 ± 65^c	34.17 ± 1.02^c	4.12 ± 0.59^b
80/20/CNa	9.14 ± 1.70^a	1373 ± 61^c	28.52 ± 0.79^d	3.04 ± 0.13^c
80/20/C30B	1.03 ± 0.16^b	1598 ± 51^b	29.24 ± 0.85^d	2.32 ± 0.09^d

^{a-d} Different letters in the same column indicate significative differences ($p < 0.05$).

grade)/PBAT Ecoflex®/Cloisite 30B (3% w/w) nanocomposites with maleic anhydride used as compatibilizer. They observed a drop in the tensile strength and elongation at break in nanocomposites beyond 15 wt% of PBAT loading as compared to the PLA matrix due to the immiscibility of the polymers and agglomeration of the clay particles in the interface, which induce cracks in the nanocomposites. This behavior in polymer/clay nanocomposites was also discussed by Jiang *et al.* [23], who observed that tensile strength and modulus of PLA Ingeo™ 4032D (extrusion grade) nanocomposites can remain unaffected or even increase only if strong polymer/organoclay interaction occurred. In the case of 80/20/C30, the stronger interaction between polymer matrix and clay C30B (discussed in Section 3.1) causes an increase in interfacial area between clay and polymer, which results in a higher amount of stress transfer between the matrix and the filler particles and an improvement in the E property of the nanocomposite.

3.5 Thermal Properties

The DSC heating curves of PLA, PBAT, 80/20 blend and its nanocomposites after melt crystallization are shown in Figure 5. Numerical values of the thermal events are shown in Table 3. The addition of PBAT to the PLA matrix resulted in a slight decrease in the T_g of the PLA component (2 °C). This decrease in T_g value (albeit small) could suggest partial miscibility of PLA and PBAT phases [20]. For nanocomposites, T_g values decreased 4 and 5 °C with CNa and C30B respectively. Clay platelets could cause some steric effects that prevent the chains from packing compactly, increasing free volume of the polymer matrix and leading to the decrease in T_g [24]. The PLA melting temperature in the blend was similar to the one of neat PLA. Regarding the nanocomposites, a slight decrease in the melting temperature of PLA was found. This effect could be due to a decrease in molar mass caused by polymer degradation during mixing [25]. Neat PLA displayed a cold crystallization exotherm at 99.8 °C; PBAT incorporation (80/20 blend) causes a decrease in this value (97.8 °C). Jiang *et al.* [2] and Quero *et al.* [20] also reported that the incorporation of PBAT Ecoflex® decreased PLA Ingeo™ (extrusion grade) cold crystallization temperature by approximately 10 °C and 7 °C respectively, indicating an enhanced crystalline ability of PLA in the blend. When CNa and organically modified C30B clays were added into 80/20 blends, a 4–5 °C shift in the cold crystallization temperature of PLA was observed. This decrease indicates that clay particles in nanocomposites act as a nucleation agent [5, 7]. Also, the PBAT has a broad melting peak located

within the cold crystallization temperature of PLA (see Figure 5) and could act as a plasticizer for PLA, enhancing its chain mobility and allowing the PLA to crystallize at lower temperatures during heating [7, 20]. Table 3 also shows the onset oxidation temperature (OOT), as a relative measure of a polymeric materials oxidative stability, at the mentioned heating rate [10]. As expected, the addition of PBAT to PLA results in an increase of the OOT value of around 20 °C in comparison to neat PLA. Clay addition led to an improvement in OOT compared to neat PLA (30 °C for CNa and 47 °C for C30B) and compared to 80/20 neat blend (9 °C for CNa and 26 °C for C30B). It is known that layered silicates enhance the thermal stability of a polymer matrix because they act as a heat barrier, which enhances the overall thermal stability of the system, as well as a barrier against oxygen and oxidation products during thermal decomposition [12, 13]. It can be concluded that the addition of clays increases the processability window of PLA/PBAT blends and the better dispersion and intercalation of organically modified clay C30B in the blend enhances this behavior.

3.6 Water Vapor Permeability (WVP)

The WVP values of neat polymers, 80/20 and its nanocomposites are also shown in Table 3. These WVP values are comparable to values reported for biodegradable PBAT films obtained via solution casting by Bastarrachea *et al.* [26], and PLA films via solution casting and cast extrusion by Rhim *et al.* [27] and Correa *et al.* [28] respectively. According to Bastarrachea *et al.* [26], one of the drawbacks of the PBAT films is its poor WVP. However, WVP of neat PLA films was not influenced significantly ($p \geq 0.05$) by the incorporation of 20% w/w of PBAT (80/20 blend). In the case of nanocomposites, the WVP changed significantly ($p < 0.05$) depending on

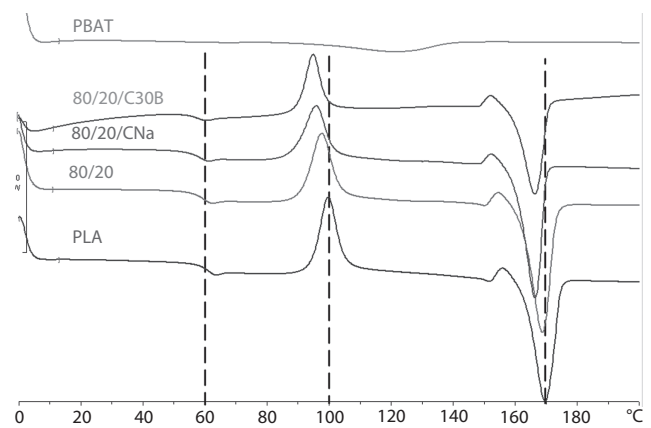


Figure 5 DSC heating curves of PLA, PBAT, 80/20 blend and its nanocomposites after melt crystallization.

Table 3 Thermal properties on second heating DSC scans and WVP of the samples.

Sample	T_g $\frac{1}{2}$ Cp ¹ (°C)	T_{cc} ² (°C)	ΔH_{cc} (J/g)	T_m ² (°C)	ΔH_m (J/g)	χ (%)	OOT ³ (°C)	WVP ⁴
PLA	60.0	99.8	26.4	168.9	39.0	13.6	190.2	1.84 ± 0.07 ^a
80/20	58.5	97.8	22.7	168.4	36.9	19.2	210.7	1.81 ± 0.09 ^a
80/20/CNa	56.7	96.1	22.1	165.9	39.3	24.3	219.3	2.22 ± 0.07 ^b
80/20/C30B	55.9	95.0	19.7	166.2	37.6	25.3	236.8	1.46 ± 0.08 ^c
PBAT	–	–	–	121.3	13.5	11.9	328.4	3.13 ± 0.03 ^d

¹T_g was determinate by the half step temperature.

²T_{cc} and T_m are taken at the maximum peak of cold crystallization and melting peaks.

³Temperature correspond to decomposition onset.

⁴WVP values are expressed in g·s⁻¹·m⁻¹·Pa⁻¹.

^{a-d}Different letters in the same column indicate significative differences ($p < 0.05$).

the type of MMT used. The WVP of nanocomposites compounded with CNa increased around 23% while films with C30B decreased 20% in comparison to the WVP of neat 80/20 films. This result could be due to the hydrophilicity of CNa, whereas the results obtained for the for 20/80C30B could be due to the hydrophobicity of organically modified clay C30B and the long and tortuous paths created by clay platelets of C30B dispersed in the polymer matrix slowing down the progress of water molecules through the matrix.

4 CONCLUSIONS

We have prepared PLA/PBAT/clay nanocomposites by melt blending of PLA, PBAT and two types of clays (unmodified and organically modified). As evidenced by XRD, an intercalated morphology was achieved with both types of clays but the extent of this intercalation was higher for the C30B-based nanocomposite. Also, the results clearly indicate that PBAT addition to PLA and the PLA flow capability seem to have no effect on the extent of polymer intercalation into the clay galleries. Further rheological studies of the particles dispersion state have confirmed that observation. The SEM images showed PLA and PBAT as immiscible polymers which formed a phase-separated morphology, but OMMT addition can reduce the coalescence of the system and the domain size of the phase-separated particles. Also, tensile modulus, crystallinity, processability window, and WVP of the matrix were enhanced with the addition of C30B. These results have confirmed that between both clays used, C30B exhibited the best interaction with a renewable and high flow PLA/PBAT polymer blend.

ACKNOWLEDGMENTS

This work was supported by Conicyt (PICT-2011-2690). Juan P. Correa acknowledges CONICET for a doctoral

scholarship. We thank Dr. Rosa Torres for assistance with DRX measurements and the Laboratory of Electronic Microscopy of INTI for evaluation of micrographs and images.

REFERENCES

1. M. Jamshidian, E.A. Tehrany, M. Imran, M. Jacquot, and S. Desobry, Poly-lactic acid: Production, applications, nanocomposites, and release studies. *Compr. Rev. Food Sci. Food Saf.* **9**, 552–571 (2010).
2. L. Jiang, M.P. Wolcott, and J. Zhang, Study of biodegradable polylactide/poly(butylene adipate-co-terephthalate) blends. *Biomacromolecules.* **7**, 199–207 (2006).
3. S.S. Ray, Recent trends and future outlooks in the field of clay-containing polymer nanocomposites. *Macromol. Chem. Phys.* **215**, 1162–1179 (2014).
4. M.A. Gunning, L.M. Geever, J.A. Killion, J.G. Lyons, B. Chen, and C.L. Higginbotham, The effect of the mixing routes of biodegradable polylactic acid and polyhydroxybutyrate nanocomposites and compatibilised nanocomposites. *J. of Thermoplast. Compos. Mater.* **29**, 538–557 (2016).
5. Z. Yu, J. Yin, S. Yan, Y. Xie, J. Ma, and X. Chen, Biodegradable poly(l-lactide)/poly(ϵ -caprolactone)-modified montmorillonite nanocomposites: Preparation and characterization. *Polymer.* **48**, 6439–6447 (2007).
6. M. Kumar, S. Mohanty, S.K. Nayak, and M. Rahail Parvaiz, Effect of glycidyl methacrylate (GMA) on the thermal, mechanical and morphological property of biodegradable PLA/PBAT blend and its nanocomposites. *Bioresour. Technol.* **101**, 8406–8415 (2010).
7. M. Shahlari and S. Lee, Mechanical and morphological properties of poly(butylene adipate-co-terephthalate) and poly(lactic acid) blended with organically modified silicate layers. *Polym. Eng. Sci.* **52**, 1420–1428 (2012).
8. A.K. Mohapatra, S. Mohanty, and S.K. Nayak, Study of thermo-mechanical and morphological behaviour of biodegradable PLA/PBAT/layered silicate blend nanocomposites. *J. Polym. Environ.* **22**, 398–408 (2014).
9. Standard test method for tensile properties of thin plastic sheeting, ASTM D 882-12 (2012).

10. Standard test methods for oxidation onset temperature of hydrocarbons by differential scanning calorimetry, ASTM E 2009-14 (2014).
11. Standard test methods for water vapor transmission of materials, ASTM E 96/E96M-15 (2015).
12. K. Fukushima, M.-H. Wu, S. Bocchini, A. Rasyida, and M.-C. Yang, PBAT based nanocomposites for medical and industrial applications. *Mater. Sci. Eng. C Mater. Biol. Appl.* **32**, 1331–1351 (2012).
13. K. Fukushima, D. Tabuani, M. Arena, M. Gennari, and G. Camino, Effect of clay type and loading on thermal, mechanical properties and biodegradation of poly(lactic acid) nanocomposites. *React. Funct. Polym.* **73**, 540–549 (2013).
14. A. Botana, M. Mollo, P. Eisenberg, and R.M. Torres Sanchez, Effect of modified montmorillonite on biodegradable PHB nanocomposites. *Appl. Clay. Sci.* **47**, 263–270 (2010).
15. J.M. Cervantes-Uc, J.V. Cauich-Rodriguez, H. Vazquez-Torres, L.F. Garfias-Mesias, and D.R. Paul, Thermal degradation of commercially available organoclays studied by TGA-FTIR. *Thermochim. Acta.* **457**, 92–102 (2007).
16. T.D. Fornes, P.J. Yoon, D.L. Hunter, H. Keskkula, and D.R. Paul, Effect of organoclay structure on nylon 6 nanocomposite morphology and properties. *Polymer.* **43**, 5915–5933 (2002).
17. M. Sabzi, L. Jiang, M. Atai, and I. Ghasemi, PLA/sepiolite and PLA/calcium carbonate nanocomposites: A comparison study. *J. Appl. Polym. Sci.* **129**, 1734–1744 (2013).
18. L.C. Arruda, M. Magaton, R.E.S. Bretas, and M.M. Ueki, Influence of chain extender on mechanical, thermal and morphological properties of blown films of PLA/PBAT blends. *Polym. Test.* **43**, 27–37 (2015).
19. D.H.S. Souza, C.T. Andrade, and M.L. Dias, Rheological behavior of poly(lactic acid)/synthetic mica nanocomposites. *Mater. Sci. Eng. C Mater. Biol. Appl.* **33**, 1795–1799 (2013).
20. E. Quero, A.J. Müller, F. Signori, M.-B. Coltelli, and S. Bronco, Isothermal cold-crystallization of PLA/PBAT blends with and without the addition of acetyl tributyl citrate. *Macromol. Chem. Phys.* **213**, 36–48 (2012).
21. G.F. Brito, P. Agrawal, E.M. Araújo, and T.J.A. Mélo, Effect of combining ethylene/methyl acrylate/glycidyl methacrylate terpolymer and an organoclay on the toughening of poly(lactic acid). *Polym. Eng. Sci.* **54**, 1922–1930 (2014).
22. M.Y. Gelfer, H.H. Song, L. Liu, B.S. Hsiao, B. Chu, M. Rafailovich, M. Si, and V. Zaitsev, Effects of organoclays on morphology and thermal and rheological properties of polystyrene and poly(methyl methacrylate) blends. *J. Polym. Sci. Pol. Phys.* **41**, 44–54 (2003).
23. L. Jiang, J. Zhang, and M.P. Wolcott, Comparison of polylactide/nano-sized calcium carbonate and polylactide/montmorillonite composites: Reinforcing effects and toughening mechanisms. *Polymer.* **48**, 7632–7644 (2007).
24. P. Krishnamachari, J. Zhang, J. Lou, J. Yan, and L. Uitenham, Biodegradable poly(lactic acid)/clay nanocomposites by melt intercalation: A study of morphological, thermal, and mechanical properties. *Int. J. Polym. Anal. Character.* **14**, 336–350 (2009).
25. K. Prakalathan, S. Mohanty, and S.K. Nayak, Reinforcing effect and isothermal crystallization kinetics of poly(3-hydroxybutyrate) nanocomposites blended with organically modified montmorillonite. *Polym. Compos.* **35**, 999–1012 (2014).
26. L. Bastarrachea, S. Dhawan, S.S. Sablani, J.-H. Mah, D.-H. Kang, J. Zhang, and J. Tang, Biodegradable poly(butylene adipate-co-terephthalate) films incorporated with nisin: Characterization and effectiveness against *Listeria innocua*. *J. Food. Sci.* **75**, E215–E224 (2010).
27. J.-W. Rhim, S.-I. Hong, and C.-S. Ha, Tensile, water vapor barrier and antimicrobial properties of PLA/nanoclay composite films. *LWT – Food. Sci. Technol.* **42**, 612–617 (2009).
28. Y.-M. Corre, S. Bruzard, J.-L. Audic, and Y. Grohens, Morphology and functional properties of commercial polyhydroxyalkanoates: A comprehensive and comparative study. *Polym. Test.* **31**, 226–235 (2012).

1
2
3
4
5
6
7
8
9
10
11
12
13
14
15
16
17
18
19
20
21
22
23
24
25
26
27
28
29
30
31
32
33
34
35
36
37
38
39
40
41
42
43
44
45
46
47
48
49
50
51
52
53
54
55

